Article

Design and Dispersion Control of Microstructured Multicore Tellurite Glass Fibers with In-Phase and Out-of-Phase Supermodes

Elena A. Anashkina * and **Alexey V. Andrianov**

Institute of Applied Physics of the Russian Academy of Sciences, 46 Ul'yanov Street, 603950 Nizhny Novgorod, Russia; andrian@ipfran.ru
* Correspondence: elena.anashkina@ipfran.ru

Abstract: High nonlinearity and transparency in the 1–5 μm spectral range make tellurite glass fibers highly interesting for the development of nonlinear optical devices. For nonlinear optical fibers, group velocity dispersion that can be controlled by microstructuring is also of great importance. In this work, we present a comprehensive numerical analysis of dispersion and nonlinear properties of microstructured two-, four-, six-, and eight-core tellurite glass fibers for in-phase and out-of-phase supermodes and compare them with the results for one-core fibers in the near- and mid-infrared ranges. Out-of-phase supermodes in tellurite multicore fibers are studied for the first time, to the best of our knowledge. The dispersion curves for in-phase and out-of-phase supermodes are shifted from the dispersion curve for one-core fiber in opposite directions; the effect is stronger for large coupling between the fields in individual cores. The zero dispersion wavelengths of in-phase and out-of-phase supermodes shift to opposite sides with respect to the zero-dispersion wavelength of a one-core fiber. For out-of-phase supermodes, the dispersion can be anomalous even at 1.55 μm, corresponding to the operating wavelength of Er-doped fiber lasers.

Keywords: microstructured fiber; tellurite glass fiber; dispersion; multicore fiber

1. Introduction

The development of fiber laser sources and fiber optical components in the near- and mid-infrared (mid-IR) ranges is an important and topical problem of modern photonics. Fiber laser systems and nonlinear optical converters are in demand for a wide variety of applied and fundamental problems, including telecommunications, noninvasive medical diagnostics, laser surgery, sensing, spectroscopy, etc. [1–15].

When designing nonlinear optical fiber devices, significant attention is paid to the control of group velocity dispersion, which is often of great importance in the development of laser sources based on supercontinuum generation, Raman solitons, and long-wavelength dispersive waves [1,16]. Microstructuring is widely used for the development of fibers with required dispersion. Ordered structures with characteristic sizes of microns or submicrons are created using air holes or glass rods [15–27]. Waveguide modes in microstructured fibers are formed as a result of the interference of waves arising from reflection and refraction at the refractive-index microinhomogeneities [18]. In addition to the widespread photonic crystal fibers, in which several regular layers of air holes or glass rods are located around the core [16,26,28], there are suspended-core fibers, in which a thin core is surrounded by one row of air holes with thin walls between them [14,26,29–35]. In addition, the manufacture of solid microstructured fibers from low-temperature chalcogenide and tellurite glasses simultaneously was reported [36].

Microstructuring can also be used to obtain multicore fibers, which is an emerging technology in fiber photonics. There exist structures formed by several regularly distributed cores with characteristic diameters of a few microns, in which the modes of individual cores

overlap [37,38]. In this case, from the solution of the Helmholtz equation, it is possible to find modes of the entire structure, which are called supermodes [38]. For the fundamental supermode with the highest effective refractive index, the fields in each core are in-phase. For multicore fibers with cores arranged in a ring, the amplitude distribution for the in-phase supermode is the same in each core due to symmetry. As a rule, in the study of multicore fibers, primary attention is paid to the in-phase supermode [37,39,40]. However, in the recent analytical, numerical, and experimental works, it has been shown that an out-of-phase supermode (in which the phases of the fields in neighboring cores differ by π) can also be of great interest due to its stability in different nonlinear regimes [41–44]. Multicore fibers allow operation with pulse energies and powers higher than those of one-core fibers [41,42,44] (however, for ultrashort pulses, spatial walk-off of supermodes should be taken into account [45,46]). In addition, the supermode dispersion can vary significantly compared to the dispersion for a one-core fiber. For example, for nano-sized photonic wires, it has been shown theoretically that the dispersion of waveguide arrays can vary dramatically between different supermodes, and anomalous dispersion can be attained in coupled waveguides while a single waveguide has normal dispersion [47], which was also confirmed experimentally [48].

An important issue is the method of supermode excitation. To excite an in-phase supermode in a silica multicore fiber, a single-core fiber can be spliced with a multicore fiber after matching their claddings [49]. More complicated fiber coupling devices, such as fan-in/fan-out fiber couplers, allowing access to one or more cores, can also be used [50]. An out-of-phase supermode can be excited with free-space objective lenses [48] or spatial light modulators [43].

For the fabrication of microstructured multicore fibers operating in the near-IR range (as well as for the fabrication of any other types of near-IR fibers), silica glasses are the most popular due to the existing advanced technologies [37]. The study of multicore fibers in the mid-IR is practically in its infancy, one of the reasons being the impossibility of using silica glasses due to high losses at wavelengths >2.3 μm. However, the development of technologies in the mid-IR range stimulates the search for new amorphous materials that combine a wide range of transparency, suitable nonlinear optical and/or laser characteristics, and optimal chemical and mechanical properties. Soft glasses, such as fluoride, tellurite, and chalcogenide, with low glass transition temperatures (~200–400 °C) are good candidates for mid-IR fiber development [26]. Tellurite glasses based on tellurium dioxide TeO_2 are transparent in the near- and mid-IR ranges (up to ~5–6 μm), have high chemical stability, and a high nonlinear refractive index [26]; therefore, they are of great interest for the design of optical elements and nonlinear optical waveguide structures, including microstructured multicore fibers. To date, several works report the manufacture and study of multicore tellurite glass fibers [51–54]. A numerical study of the dispersion of the fundamental supermode was carried out in [53,54]. However, we are not aware of the study of the dispersion and nonlinear properties of an out-of-phase supermode in multicore fibers based on tellurite glasses.

In this work, we present a comprehensive numerical analysis of the dispersion and nonlinear properties of microstructured multicore tellurite glass fibers for in-phase and out-of-phase supermodes and compare them with the results for one-core fibers in the near- and mid-IR ranges. The out-of-phase supermodes in multicore tellurite fibers are studied for the first time, to the best of our knowledge.

2. Materials and Methods

2.1. Materials

Here, we considered tungstate-tellurite glass with the addition of lanthanum dioxide as the core glass. The advantages of such glasses are high glass transition temperature, stability against crystallization, low thermal expansion coefficient, and a wide transparency range of ~0.5 to 5.5 μm [55–57]. For a slight change in the refractive index in the fabrication of step-index fibers, the content of oxides can be slightly varied without deteriorating the

physicochemical glass properties [57]. Modern technologies of deep dehydration of TeO_2-WO_3-La_2O_3 glasses make it possible to obtain an extremely low content of hydroxyl groups (5.5×10^{15} cm^{-3}, the corresponding volume absorption coefficient is ~0.001 cm^{-1} [57]), which significantly reduces optical losses in the wavelength range of about 3 μm. In addition, TeO_2-WO_3-La_2O_3 glasses have a large value of the nonlinear refractive index ($n_2 = 6.9 \times 10^{-19}$ m^2/W), more than 20 times higher than that for silica glass [56], which is important for the nonlinear optical conversion of radiation in the mid-IR range, including the generation of supercontinuum, Raman solitons, long-wavelength dispersive waves, etc. [1]. Moreover, TeO_2-WO_3-La_2O_3 glasses are compatible with many other glasses with significantly different refractive indices (have similar thermal properties), which makes it possible to produce fibers with dispersion strongly different from material dispersion [56] due to a large waveguide contribution.

We studied two cases of core/cladding glasses: in the first case, the difference between the refractive indices of the cores and the cladding (dn) was small, equal to 0.3% of the refractive index of the core, and in the second case, the difference was very large, amounting to almost 20%. For a small difference in the refractive indices between the core and the cladding, the waveguide contribution leads to a shift of the zero-dispersion wavelength (ZDW) to a longer wavelength compared to the material ZDW, while for a large difference in the refractive indices, the waveguide contribution can lead to a ZDW shift to a shorter wavelength [56] and also to the formation of group velocity dispersion curves with two ZDWs [58]. The use of microstructuring, including the creation of multicore structures, gives additional opportunities for controlling the dispersion dependences. In both cases, we considered the core glass with the 69TeO$_2$–23WO$_3$–8La$_2$O$_3$ (TWL) composition [56]. In the first case (dn = 0.3%), a glass with a composition close to TWL was taken as the cladding glass; we denoted it TWL2. In the second case for d$n \approx$ 20%, the 47.5GeO$_2$−17.5TeO$_2$−20ZnO−15Na$_2$O (GTZN) glass [56] was used. The choice of this cladding glass was due to its physical compatibility with TWL in producing step-index fibers, which was experimentally demonstrated in [56]. TWL and GTZN glasses have glass transition temperatures T_g of 425 and 401 °C, onset of crystallization temperatures T_x of 660 and 565 °C, thermal expansion coefficients of 12.8 and 11.8 ppm/°C, and softening points T_s of 412 and 442 °C, respectively [56]. Refractive indices n for TWL and GTZN glasses depending on wavelength λ were determined by the Sellmeier formula [56]:

$$n^2 = B + \frac{C_1}{\left(1 - \frac{D_1}{\lambda^2}\right)} + \frac{C_2}{\left(1 - \frac{D_2}{\lambda^2}\right)}, \tag{1}$$

with constants B, C_1, C_2, D_1, and D_2 given in Table 1.

Table 1. Sellmeier constants for 69TeO$_2$–23WO$_3$–8La$_2$O$_3$ (TWL) and 47.5GeO$_2$−17.5TeO$_2$−20ZnO−15Na$_2$O (GTZN) glasses.

Glass	B	C_1	C_2	D_1, μm^2	D_2, μm^2
TWL	2.225	2.009	1.475	0.04767	149.20
GTZN	1.679	1.292	0.500	0.03045	149.50

The refractive index of TWL2 was set to be 0.997 of the TWL refractive index. The refractive indices of the considered glasses are shown in Figure 1a, and the calculated material dispersions ($\beta_2 = \partial^2(n \cdot \omega/c)/\partial\omega^2$, where $\omega = 2\pi c/\lambda$ is the angular frequency, and c is the speed of light [1]) in Figure 1b. The material dispersion of the glasses is also shown in Figure 1c but at a magnified scale near ZDWs. Note that the ZDWs of TWL and GTZN are about 2.2 μm and 2.3 μm, respectively.
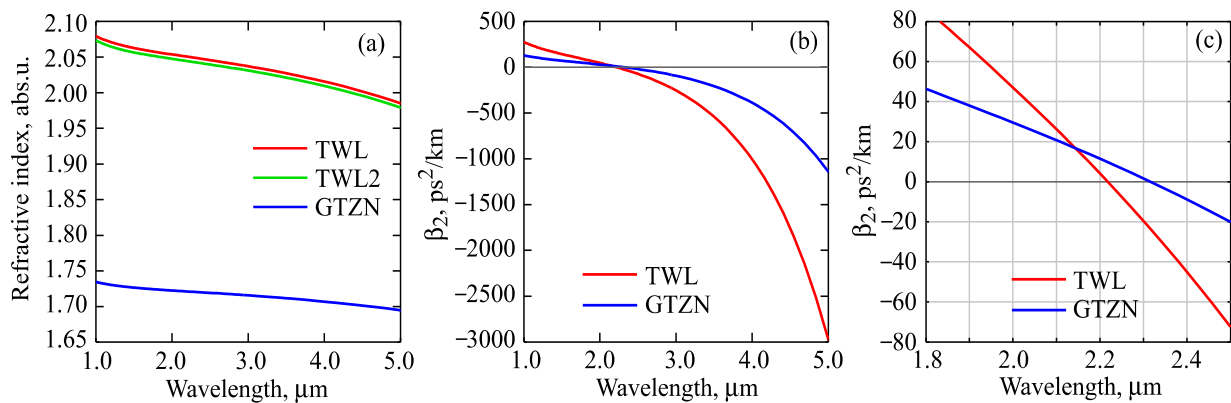
Figure 1. (**a**) Refractive indices of TWL, TWL2, and GTZN glasses calculated from Equation (1) using the Sellmeier constants from Table 1. Calculated dispersion of TWL and GTZN glasses in a wide wavelength range (**b**) and near ZDWs (**c**).

2.2. Fiber Geometry and Mode Structures

Let us now study step-index one-core fibers, two-core fibers, and multicore fibers with 4, 6, and 8 cores arranged in a ring. The diameter of each individual core is denoted by *d* and the distance between the cores by *L* (Figure 2). The diameter of the cladding was not very important, but it should be at least 120–150 μm not to affect the distribution of the mode fields in the cores and to ensure sufficient mechanical strength of the fiber. For step-index one-core fibers, we considered only the fundamental HE_{11} mode. For *N*-core fibers (*N* = 2, 4, 6, 8), we studied supermodes with in-phase and out-of-phase field distributions. We did not analyze the possibility of exciting higher modes in each individual core (which is possible if the *V*-parameter is larger than 2.405 [1]). The problem of one-core fibers can be of independent interest since, for their certain parameters, the dispersion can be changed significantly in comparison with the material dispersion. In addition, by comparing the results obtained for multicore fibers with the ones obtained for one-core fibers, we could analyze the contribution of core coupling to dispersion characteristics and formulate fairly general conclusions.
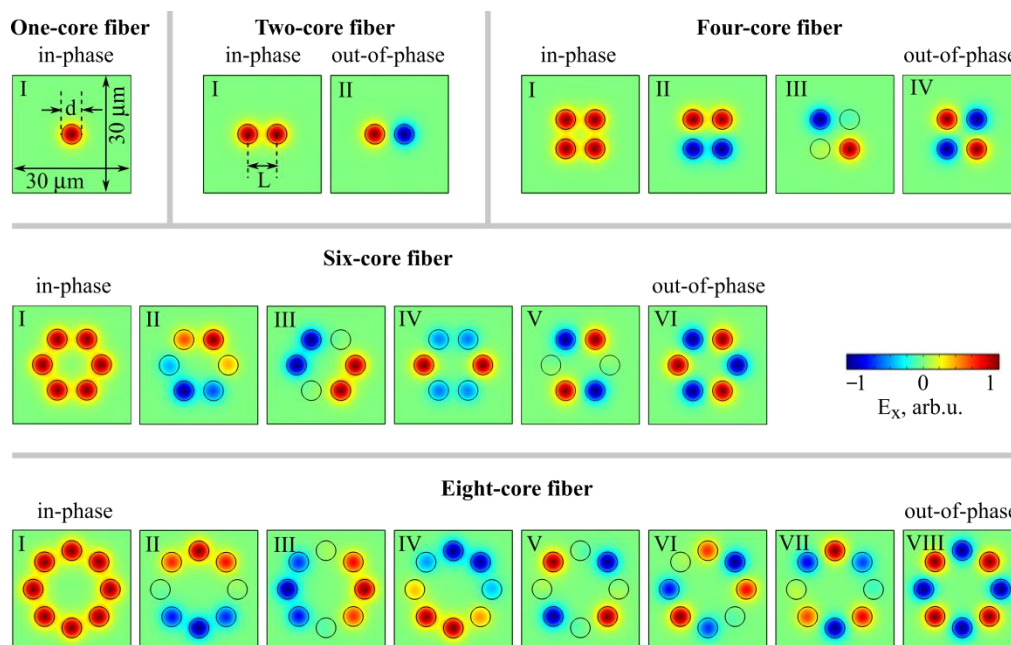

Figure 2. Examples of the fundamental mode field for a one-core fiber and fields of supermodes for two-core, four-core, six-core, and eight-core fibers. All calculations were made for TWL/TWL2 core/cladding glasses, *d* = 10 μm, *L* = 15 μm at a wavelength of 2 μm. The color bar shown near the six-core fiber is the same for all fibers.

For an *N*-core fiber, there are *N* supermodes [38], the lowest (fundamental) of which with the maximum effective refractive index corresponds to the in-phase field distribution, and the highest one with the minimum effective refractive index corresponds to the out-of-phase field distribution. Examples of field distributions in fibers with a different number of cores are demonstrated in Figure 2. Note that many supermodes, differing from the fundamental and the highest ones, were degenerate with respect to the effective refractive index (for example, II and III for a four-core fiber) [38], so their use was impractical. In addition, for supermodes with intermediate values of effective refractive indices, the field intensities in some cores can differ significantly from the maximum and even be equal to zero. For in-phase and out-of-phase supermodes, the intensities in each core were maximized, which is most practical for applications.

2.3. Numerical Methods

For one-core step-index fibers, we used the following simple approach to find effective refractive indices n_{eff} and field distributions of the fundamental propagating modes. It is well-known that for an axially symmetric core, the characteristic equation obtained based on Maxwell's equations using the boundary conditions for the tangential field components for the HE$_{11}$ mode can be written in the form [59]:

$$\left[\frac{J_1'(U)}{U J_1(U)} + \frac{K_1'(W)}{W K_1(W)} \right] \left[\frac{J_1'(U)}{U J_1(U)} + \left(\frac{n_{Clad}}{n_{Core}} \right)^2 \frac{K_1'(W)}{W K_1(W)} \right] = \left(\frac{1}{U^2} + \frac{1}{W^2} \right) \left[\frac{1}{U^2} + \left(\frac{n_{Clad}}{n_{Core}} \right)^2 \frac{1}{W^2} \right], \tag{2}$$

where

$$U = \frac{d}{2} \sqrt{k_0^2 n_{Core}^2 - \beta^2}, \; W = \frac{d}{2} \sqrt{\beta^2 - k_0^2 n_{Clad}^2}, \tag{3}$$

J_1 is the Bessel function of the 1st kind of the 1st order, K_1 is the modified Bessel function of the 2nd kind (Macdonald function) of the 1st order, the prime denotes differentiation with respect to the argument, $k_0 = \omega/c$, $\beta = n_{eff}\omega/c$, n_{Core} and n_{Clad} are refractive indexes of core and cladding glasses described in Section 2.1. The results obtained by this method for a set of fiber parameters were compared with the results obtained by a finite element simulation in the program COMSOL. We found a perfect agreement between them, which confirmed the correctness of our simulation based on homemade computer code.

To investigate the properties of microstructured multicore fibers described within the framework of the Maxwell system of equations [59], we performed numerical simulations in COMSOL. We found effective refractive indices n_{eff} for all supermodes and their field distributions.

The dispersion β_2 for one-core and microstructured multicore fibers was calculated as

$$\beta_2 = \frac{\partial^2 \left(\frac{\omega}{c} \text{Re}\left(n_{eff} \right) \right)}{\partial \omega^2}, \tag{4}$$

where $\text{Re}(n_{eff})$ is the real part of the effective refractive index.

We also calculated nonlinear fiber characteristics. We calculated the effective mode field areas as

$$A_{eff} = \frac{\left(\int P_z d^2 r \right)^2}{\int P_z^2 d^2 r}, \tag{5}$$

where the *z*-component of the Poynting vector is P_z, and *r* is the coordinate in the plane normal to the *z*-direction [59].

The nonlinear Kerr coefficient is defined as

$$\gamma = \frac{2\pi}{\lambda} \frac{\int n_2 P_z^2 d^2 r}{\left(\int P_z d^2 r \right)^2}, \tag{6}$$

here n_2 is the nonlinear refractive index; $n_2 = 6.9 \times 10^{-19}$ m^2/W for TWL and $n_2 = 2.1 \times 10^{-19}$ m^2/W for GTZN glasses [56].

3. Results

3.1. One-Core Fibers

First of all, we analyzed one-core step-index fibers. In the case of TWL/TWL2 core/cladding glasses, we considered core diameters in the 7–12 μm range, reasonable at a small dn. Figure 3a shows the simulated dispersion. For this case, there was only one ZDW, slightly shifted from the material ZDW. The ZDW position for the considered fiber diameters is shown in Figure 3a by a solid black line. The thinner the core, the farther the ZDW was shifted to longer wavelengths due to the larger waveguide contribution. The thicker the core, the closer the fiber dispersion to the material one. For example, ZDW = 2.34, 2.25, 2.23 μm for d = 7, 10, 12 μm, respectively.
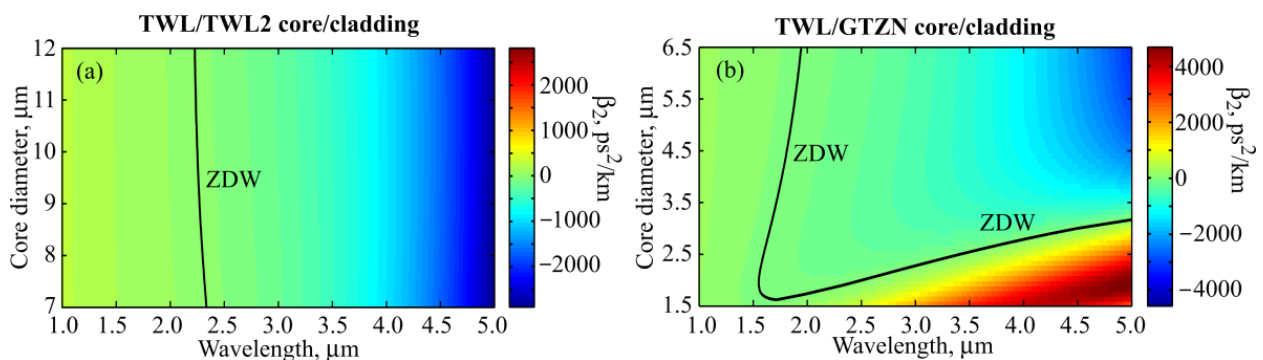

Figure 3. The calculated dispersion for one-core fibers with different core diameters for TWL/TWL2 core/cladding glasses (**a**) and TWL/GTZN core/cladding glasses (**b**).

In the case of TWL/GTZN core/cladding glasses with a large dn value, we investigated thinner core diameters in the 1.5–6.5 μm range. The simulated dispersion is demonstrated in Figure 3b. For minimal diameters of about 1.5 μm, the dispersion was completely normal in the considered wavelength range of 1–5 μm. Starting from a diameter of 1.7 μm, two ZDWs appeared one of which was always shorter than the material ZDW. The second ZDW for small core diameters was shorter than the material ZDW, but with an increase in d, it shifted significantly to the long-wavelength range. So, for d = 3.1 μm, the second ZDW was 4.75 μm. For $d \geq 3.2$ μm, only the first ZDW remained in the wavelength range of 1 to 5 μm. Note that at a wavelength of about 2 μm, where standard Tm:fiber lasers operate, the dispersion was anomalous for $d \geq 1.8$ μm, which may be important for nonlinear optical pulse conversion and design of photonic devices.

Next, we calculated effective mode field areas and nonlinear Kerr coefficients. The wavelength dependences are plotted in Figure 4a,b for TWL/TWL2 core/cladding glasses and in Figure 4c,d for TWL/GTZN core/cladding glasses. In the near-IR range, the mode field for both TWL/TWL2 and TWL/GTZN core/cladding glass fibers was fairly well localized near the core. Therefore, the larger the core diameter, the larger the effective mode field area and the lower the nonlinear Kerr coefficient were. However, with an increase in the wavelength, differences in the qualitative behavior of these functions for two kinds of fibers were observed. For TWL/TWL2 core/cladding fibers, starting from $\lambda \sim 2.5$ μm, a relatively thin core with a small dn could no longer confine the mode sufficiently well, so its field area started to increase significantly with an increase in λ. Whereas for larger values of d, the mode was still localized near the core. Therefore, at the wavelengths $\lambda > 3$ μm for TWL/TWL2 core/cladding fibers, the following behavior was observed: the smaller the core diameter, the larger the effective mode area, and the lower the nonlinear Kerr coefficient is (Figure 4a,b). For TWL/GTZN core/cladding fibers, the mode is localized quite well, even for $d \geq 3$ μm, which can be seen in Figure 4c. But at smaller d at the wavelengths $\lambda > 4$ μm, the mode is poorly confined, and the effective mode area begins to increase quickly, crossing the curves for other d.

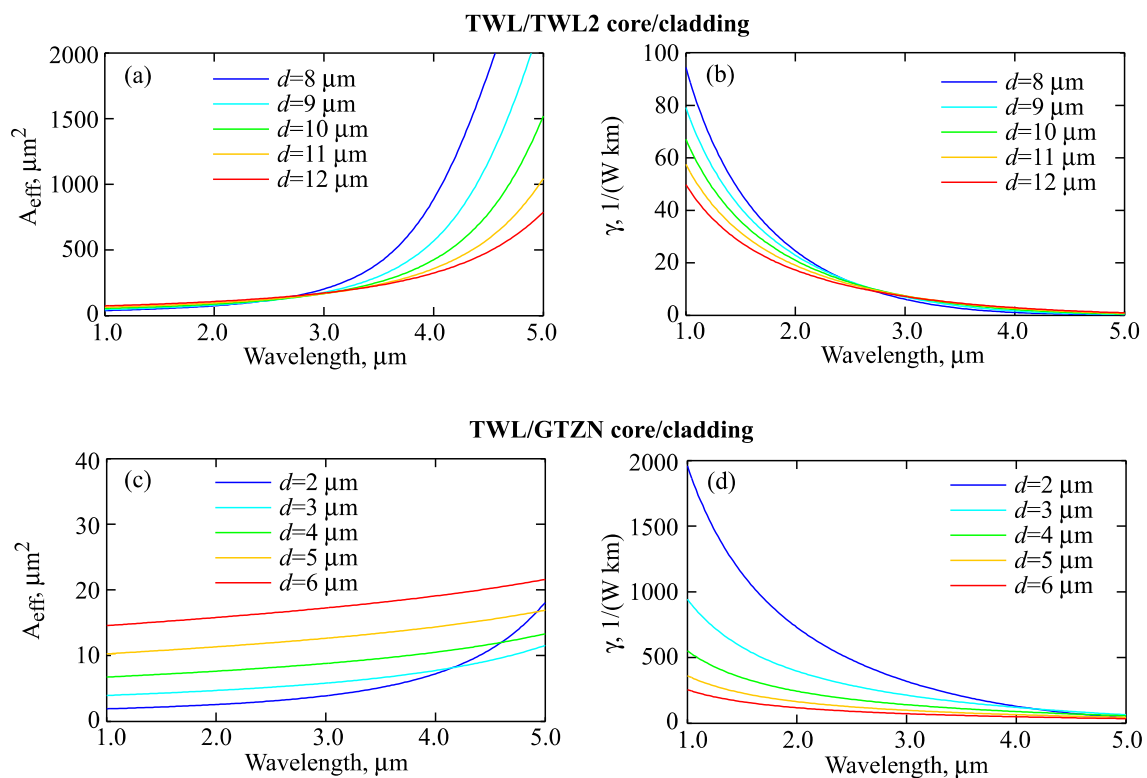**TWL/TWL2 core/cladding**

TWL/GTZN core/cladding

Figure 4. The calculated effective mode field areas A_{eff} and nonlinear Kerr coefficients γ for one-core fibers with different core diameters for TWL/TWL2 core/cladding (**a**,**b**) and for TWL/GTZN core/cladding (**c**,**d**).

3.2. Mode Coupling in Two-Core Fibers

Now consider the mode coupling of optical signals propagating in two closely spaced cores. Hereinafter, we investigated TWL/TWL2 core/cladding fibers with d = 10 μm (for other diameters, the patterns are similar). For TWL/GTZN core/cladding fibers, we studied two options for the diameter d = 2 μm and d = 3 μm, since in some cases discussed below, there were qualitative differences between them. The schematic diagram is shown in Figure 5a. The fundamental modes propagating in cores with diameters d and distance L between the centers of the cores overlapped and interacted. The coupling coefficients were calculated as in [1] and plotted as functions of wavelength for different L/d ratios in Figure 5b for TWL/TWL2 core/cladding fibers and in Figure 5c,d for TWL/GTZN core/cladding fibers. The coupling coefficients were higher at longer wavelengths due to larger mode field areas (Figure 4a,c). As expected, the closer the cores, the higher the coupling coefficient.

3.3. Multicore Fibers with Different Numbers of Cores and Constant L/d Ratio

When considering multicore fibers, the mode field in each core is coupled with mode fields propagating in the remaining N—1 cores. For each core, the coupling is maximal with the two nearest neighbors (or with one in the case of two-core fibers) since the distance to them is minimal. The coupling coefficient, as shown in Section 3.2, was strongly dependent on a distance between the cores. For a four-core fiber, the distances from the center of the selected core to the others are L, L, and $2^{1/2} \cdot L$. For the six-core fibers, the distances are L, L, $3^{1/2} \cdot L$, $3^{1/2} \cdot L$, and $2L$. With an increase in the number of cores, coupling with the other neighbors becomes increasingly less significant. We investigated multicore fibers with N = 2, 3, 6, and 8. Six-core fibers are quite popular, and fibers with $N \geq 8$ are rarely used. For N-core fibers with N = 10, 12, ... cores arranged in a ring, it is expected that the dispersion properties will be practically the same as for eight-core fibers, since the

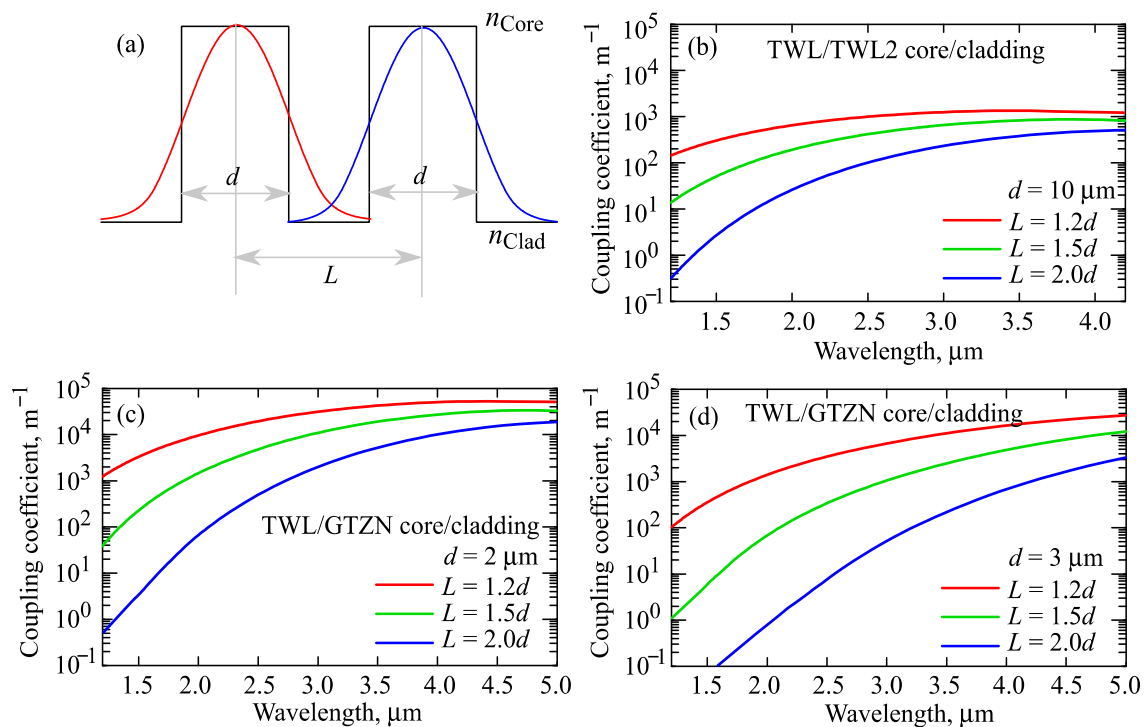distances to cores located across one are quite similar and coupling with farther cores can be neglected.

Figure 5. Schematic diagram demonstrating mode field overlapping in a two-core fiber (**a**). Calculated coupling coefficients for two-core fibers with different L/d ratios for TWL/TWL2 core/cladding, d = 10 µm (**b**); TWL/GTZN core/cladding, d = 2 µm (**c**); TWL/GTZN core/cladding, d = 3 µm (**d**).

We simulated the dispersion for the in-phase and out-of-phase supermodes of multicore fibers with L = 1.5d (Figure 6) and compared with the simulated results for the one-core fiber plotted by bold red lines. The results for TWL/TWL2 core/cladding with d = 10 µm in a wide wavelength range and at a magnified scale near ZDWs are shown in Figure 6a,b, respectively. It was observed that the coupling between the modes of each individual core, in this case, made only a minor contribution. For in-phase supermodes, the dispersion curves were shifted slightly upwards, and the ZDW was slightly shifted towards longer wavelengths relative to the dispersion curve for the one-core fiber. For out-of-phase supermodes, the dispersion curves were shifted slightly downwards, and the ZDW was slightly shifted towards shorter wavelengths relative to the dispersion curve for the one-core fiber. The results obtained for six- and eight-core fibers practically coincided (the corresponding curves were indistinguishable in the graphs). For the in-phase supermode with N = 4, the result also coincided with the results for N = 6 and 8, but for the out-of-phase supermode with N = 4, there was a slight difference from the results obtained for out-of-phase supermodes with N = 6 and 8. The fact that the results for N = 2 differed from the others can be explained very simply by the presence of only one nearest neighboring core rather than two, in contrast to the other N.
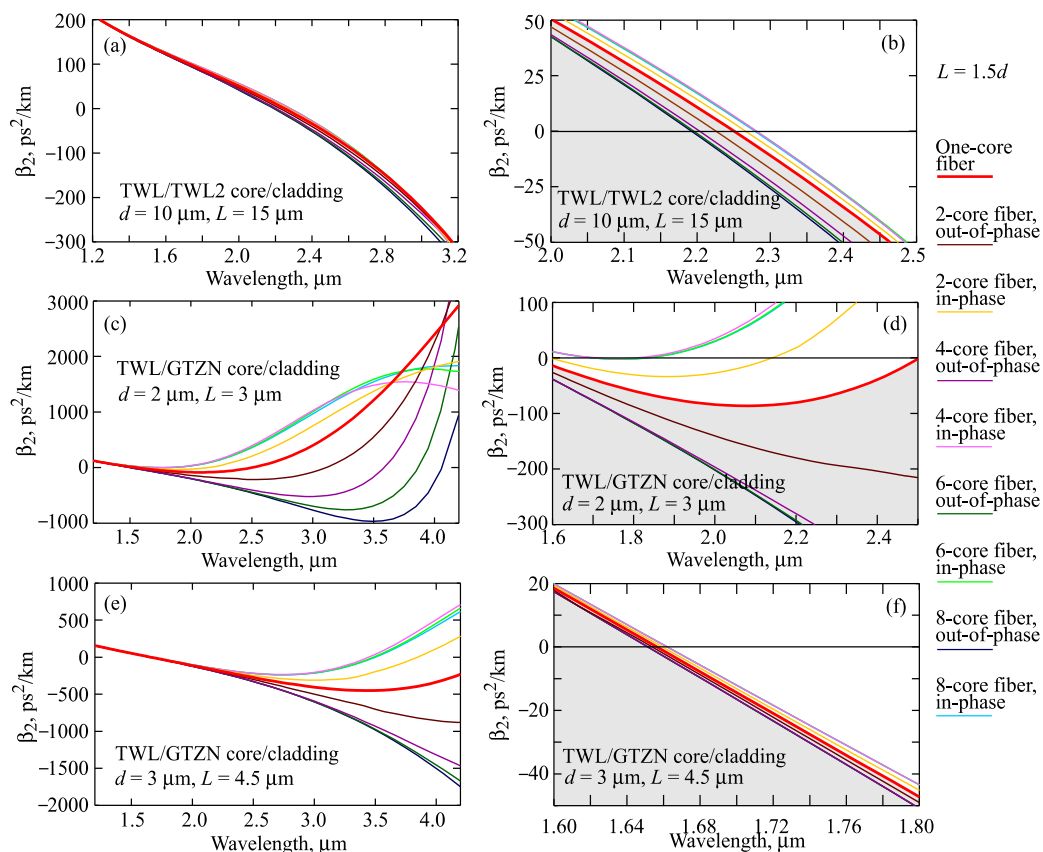
Figure 6. The calculated dispersion in wide wavelength ranges (left column) and at magnified scales near ZDWs (right columns) for fibers with a different number of cores with $L = 1.5d$ for TWL/TWL2 core/cladding with $d = 10$ μm (**a**,**b**); for TWL/GTZN core/cladding with $d = 2$ μm (**c**,**d**); and for TWL/GTZN core/cladding with $d = 3$ μm (**e**,**f**). In the right column, the dispersion curves for out-of-phase supermodes are located in the gray areas under the dispersion curves for one-core fibers.

Next, the dispersion curves for TWL/GTZN core/cladding fibers with $d = 2$ μm and $N = 1, 2, 4, 6,$ and 8 in a wide wavelength range and at a magnified scale near ZDWs are potted in Figure 6c,d, respectively. Here, the dispersions for multicore fibers were significantly different from the dispersion for one-core fibers since the coupling coefficients, as demonstrated in Section 3.2, were an order of magnitude higher than the values for the TWL/TWL2 core/cladding fiber. At wavelengths $\lambda < 3$ μm, the curves for six- and eight-core fibers practically coincided for both in-phase and out-of-phase supermodes, respectively. At $\lambda > 3.5$ μm, the mode fields were poorly localized near each core and strongly interacted not only with the nearest neighbors but also with more distant cores; therefore, the difference in the behavior of the curves was more pronounced. Atv $\lambda < 3.5$ μm, the dispersion curves for in-phase supermodes lay above, and for out-of-phase supermodes below the dispersion curve for the one-core fiber. In Figure 6d, the curves for out-of-phase supermodes are in the gray area. For in-phase supermodes, the distance between ZDWs decreased: The first ZDW was red-shifted, and the second ZDW was blue-shifted. An interesting feature was that in the wavelength range of 1.65 μm $< \lambda <$ 1.85 μm, the dispersion for in-phase supermodes in four-, six-, and eight-core fibers was flat and almost zero.

The dispersion curves for TWL/GTZN core/cladding fiber with $d = 3$ μm in a wide wavelength range and at a magnified scale near ZDWs are plotted in Figure 6e,f, respectively. The dispersion curves for six- and eight-core fibers were located very close to each other for the same supermodes over the entire wavelength range since the fields were confined strongly compared to the fibers with $d = 2$ μm. As before, the gray area in

Figure 6f contains the dispersion curves for out-of-phase supermodes. The shortwave ZDWs, as seen in Figure 6f, was about 1.66 μm. For out-of-phase supermodes, there was only one ZDW in the considered range of 1.2 to 4.2 μm, while for in-phase supermodes, there were two ZDWs.

3.4. Six-Core Fibers

We examined the influence of the distance between the cores on the dispersion and nonlinear characteristics of six-core fibers. We took the values L/d = 1.2, 1.5, and 2. The results of dispersion calculations for TWL/TWL2 core/cladding fibers with d = 10 μm are presented in Figure 7a. It was observed that for all L/d ratios, the curves were located quite close to each other. The dispersion curves for TWL/GTZN core/cladding fibers with d = 3 μm are shown in Figure 7b. Here, the difference between the results for different L/d was quite pronounced. The lower the L/d ratio, the more the dispersion curves for the six-core fiber differ from the calculated results for the one-core fiber. The dispersions for TWL/GTZN core/cladding fibers with d = 2 μm over a wide wavelength range and at a magnified scale near the ZDWs are plotted in Figure 7c,d, respectively. Here, the difference in the behavior of the curves was even more pronounced in comparison with Figure 7b. For $L/d \leq 1.5$ for an out-of-phase supermode, the dispersion was anomalous even around 1.55 μm, where standard erbium-doped fiber lasers can be used. At the same time, for an in-phase supermode, for small L/d, the dispersion was normal in the entire considered range.
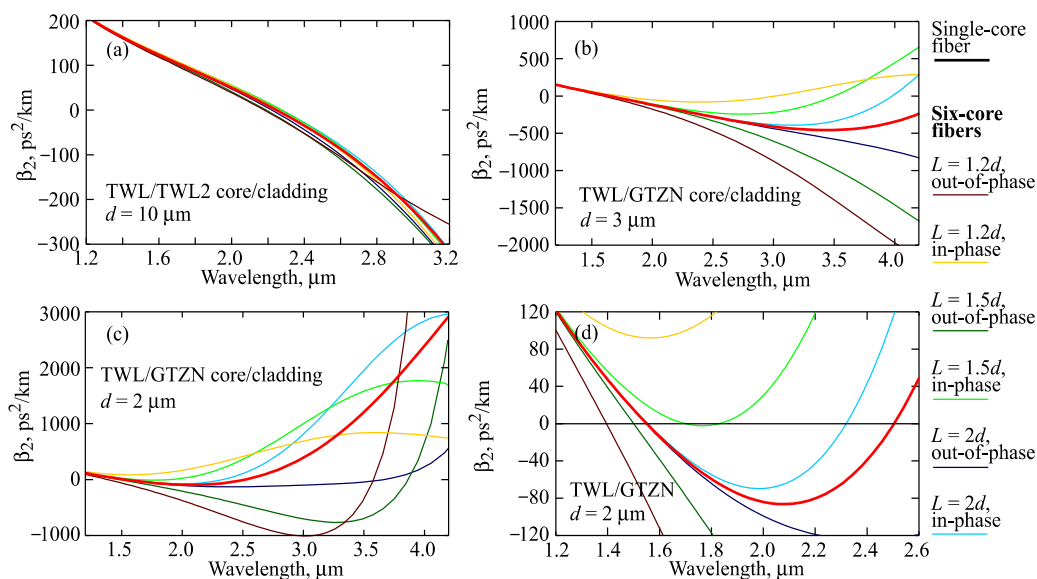

Figure 7. The calculated dispersion for six-core fibers with different L/d ratios compared to the dispersion of one-core fibers for TWL/TWL2 core/cladding with d = 10 μm (**a**); for TWL/GTZN core/cladding with d = 3 μm (**b**); and for TWL/GTZN core/cladding with d = 2 μm in a wide wavelength range (**c**) and at a magnified scale near ZDWs (**d**).

The effective mode field areas (left column) and nonlinear Kerr coefficients (right column) for TWL/TWL2 core/cladding fibers with d = 10 μm are demonstrated in Figure 8a,b, for TWL/GTZN core/cladding fibers with d = 2 μm in Figure 8c,d and for TWL/GTZN core/cladding fibers with d = 3 μm in Figure 8e,f. The differences in the curve behavior were more noticeable for longer wavelengths.
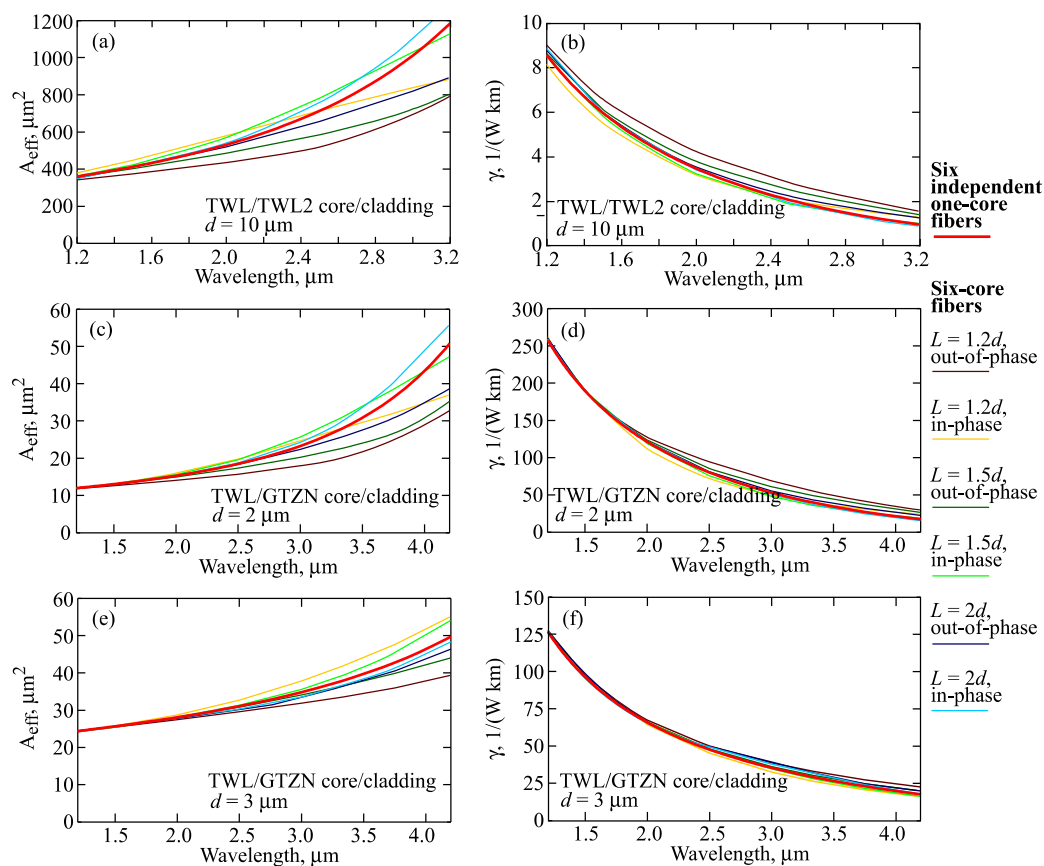
Figure 8. The calculated effective mode field areas (left column) and nonlinear Kerr coefficients (right column) for six-core fibers with different L/d ratios compared to the same for six independent cores for TWL/TWL2 core/cladding with $d = 10$ μm (**a**,**b**); for TWL/GTZN core/cladding with $d = 2$ μm (**c**,**d**); and for TWL/GTZN core/cladding with $d = 3$ μm (**e**,**f**).

To qualitatively explain the dependences observed in the left column in Figure 8, we considered the structure of the supermode fields at two different wavelengths (2 and 4 μm) for two different distances between the cores ($L = 1.2d$ and $L = 2d$). We chose TWL/GTZN core/cladding fibers with $d = 2$ μm. In Figure 9, the top row corresponded to the field structures of the in-phase and out-of-phase supermodes simulated at a wavelength of 2 μm. Figure 9 also shows for comparison the structure of the field in a one-core fiber. It is observed that the fields were well localized near the core, and their structure was practically preserved even at $L = 1.2d$. Therefore, the mode fields calculated for six-core fibers with different L/d values almost coincided with the results of the calculations for six independent cores. For $\lambda < 2$ μm, the mode was localized even better, so the graphs of the functions $A_{eff}(\lambda)$ became indistinguishable. At longer wavelengths, the structure of the fields in each core was strongly deformed. The field structures of the in-phase and out-of-phase supermodes simulated at a wavelength of 4 μm are demonstrated in the bottom row in Figure 9. It is observed that the change in the out-of-phase supermode structure was more significant than for the in-phase one. The field was pushed towards the periphery of the structure. Therefore, the largest deviations from the effective field of six independent cores were observed for the out-of-phase supermode at the minimal L/d ratio.
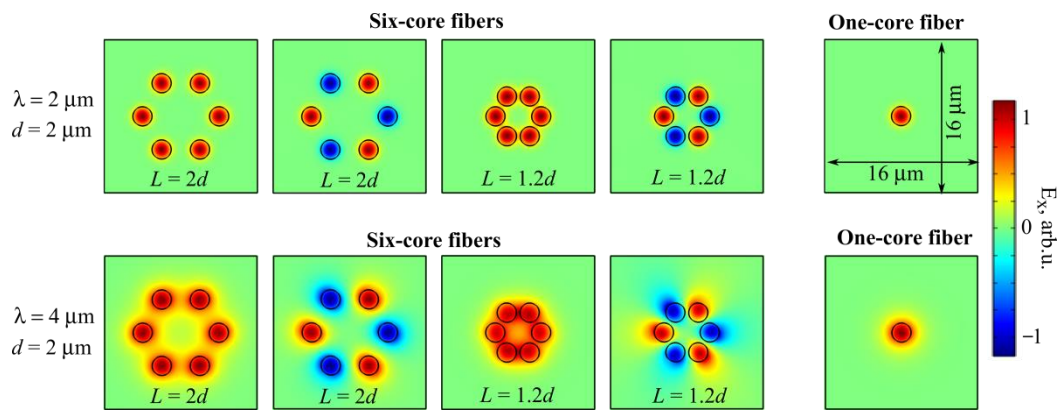
Figure 9. The fields of in-phase and out-of-phase supermodes for six-core fibers with different L/d ratios and the fundamental mode field of a one-core fiber calculated at a wavelength of 2 μm (upper row) and a wavelength of 4 μm (lower row). All results are obtained for TWL/GTZN core/cladding glasses, $d = 2$ μm.

4. Discussion and Conclusions

In this work, we calculated the dispersion and nonlinear characteristics of tellurite glass microstructured multicore fibers in the near- and mid-IR using the full-vector finite-element method. The choice of glasses for cores and cladding was based on the compatibility of their physicochemical properties suitable for manufacturing fibers [56]. The numerical analysis presented in this work showed that the dispersion of multicore fibers could be effectively controlled by fitting the following parameters: core diameters, distance between centers, number of cores, as well as by choosing the operating supermode (in-phase or out-of-phase). Note that in the previous works devoted to multicore tellurite glass fibers, the out-of-phase supermode was not investigated, but numerical studies of dispersion of in-phase supermode have been reported [53,54].

The fields propagating in individual cores overlapped and interacted, thus making a contribution to the dispersion of supermodes. Coupling coefficients were larger at longer wavelengths due to larger mode field areas. The closer the cores, the larger the coupling coefficient. So, dispersion as a function of wavelength for microstructured multicore fibers can differ significantly compared to the one-core fibers. Effective mode field areas and nonlinear Kerr coefficients of N-core fibers did not dramatically differ from the same characteristics of N independent one-core fibers (the corresponding values differ by no more than 1.5 times). The differences in the curve behavior were more noticeable for longer wavelengths.

For fibers with similar refractive indices of cores and cladding glasses (in this work, dn was 0.3%), the dispersion of individual one-core fibers did not differ much from the material dispersion. The microstructured multicore geometry made the following contribution: a single ZDW shifted toward longer wavelengths for in-phase supermodes and toward shorter wavelengths for out-of-phase supermodes compared to one-core fibers. The value of this ZDW shift was several tens of nm (up to ~100 nm).

With the use of fibers made of glasses with strongly different refractive indices of cores and cladding (in this work dn was almost 20%) with sufficiently thin cores of 2–3 μm, it was possible to achieve different qualitative and quantitative values of the group velocity dispersion in the near—and mid-IR ranges. For one-core fibers with such core properties, the dispersion already contained two ZDWs: The first ZDW was <2 μm and the second ZDW was >2.5 μm. For in-phase supermodes, the wavelength difference between the ZDWs decreased: The short-wavelength ZDW shifted to a longer wavelength, and the long-wavelength ZDW shifted to a shorter wavelength. For thin, closely spaced cores, there may arise a situation when ZDWs disappear, and the dispersion becomes all-normal. For out-of-phase supermodes, the wavelength difference between the ZDWs increased: the short-wavelength ZDW shifted to a shorter wavelength, and the long-wavelength ZDW

shifted to a longer wavelength (or completely vanished). For out-of-phase supermodes, anomalous dispersion can be attained even at 1.55 μm, where standard Er-doped fiber lasers operate. This may be useful for the development of mid-IR sources utilizing a standard near-IR pump for supercontinuum generation, soliton self-frequency shift, etc.

The results of this work can be useful both for the design and development of dispersion-controlled microstructured multicore tellurite fibers and for the development of fibers based on other glasses. The presented qualitative conclusions about the behavior of dispersion curves for in-phase and out-of-phase supermodes can be used as a basis for choosing parameters of other pairs of glasses to obtain the desired dispersion characteristics.

Author Contributions: Conceptualization, E.A.A. and A.V.A.; methodology, E.A.A.; software, E.A.A.; validation, E.A.A.; formal analysis, E.A.A.; investigation, E.A.A.; writing—original draft preparation, E.A.A.; writing—review and editing, A.V.A.; visualization, E.A.A. All authors have read and agreed to the published version of the manuscript.

Conflicts of Interest: The authors declare no conflict of interest.

References

1. Agrawal, G.P. *Nonlinear Fiber Optics*, 6th ed.; Elsevier: Amsterdam, The Netherlands, 2019.
2. Agrawal, G.P. *Applications of Nonlinear Fiber Optics*; Academic Press: London, UK, 2001.
3. Fermann, M.E.; Hartl, I. Ultrafast fiber laser technology. *IEEE J. Sel. Topics Quantum Electron.* **2009**, *15*, 191–206. [CrossRef]
4. Shi, W.; Fang, Q.; Zhu, X.; Norwood, R.A.; Peyghambarian, N. Fiber lasers and their applications. *Appl. Opt.* **2014**, *53*, 6554–6568. [CrossRef] [PubMed]
5. Bronnikov, K.; Wolf, A.; Yakushin, S.; Dostovalov, A.; Egorova, O.; Zhuravlev, S.; Semjonov, S.; Wabnitz, S.; Babin, S. Durable shape sensor based on FBG array inscribed in polyimide-coated multicore optical fiber. *Opt. Express* **2019**, *27*, 38421–38434. [CrossRef] [PubMed]
6. Supe, A.; Zakis, K.; Gegere, L.; Redka, D.; Porins, J.; Spolitis, S.; Bobrovs, V. Raman Assisted Fiber Optical Parametric Amplifier for S-Band Multichannel Transmission System. *Fibers* **2021**, *9*, 9. [CrossRef]
7. Braunfelds, J.; Senkans, U.; Skels, P.; Janeliukstis, R.; Salgals, T.; Redka, D.; Lyashuk, I.; Porins, J.; Spolitis, S.; Haritonovs, V.; et al. FBG-Based Sensing for Structural Health Monitoring of Road Infrastructure. *J. Sens.* **2021**, *2021*, 8850368. [CrossRef]
8. Kozdrowski, S.; Żotkiewicz, M.; Sujecki, S. Ultra-Wideband WDM Optical Network Optimization. *Photonics* **2020**, *7*, 16. [CrossRef]
9. Supe, A.; Olonkins, S.; Udalcovs, A.; Senkans, U.; Mūrnieks, R.; Gegere, L.; Prigunovs, D.; Grube, J.; Elsts, E.; Spolitis, S.; et al. Cladding-Pumped Erbium/Ytterbium Co-Doped Fiber Amplifier for C-Band Operation in Optical Networks. *Appl. Sci.* **2021**, *11*, 1702. [CrossRef]
10. Sojka, L.; Pajewski, L.; Lamrini, S.; Farries, M.; Benson, T.M.; Seddon, A.B.; Sujecki, S. Experimental Investigation of Actively Q-Switched Er^{3+}: ZBLAN Fiber Laser Operating at around 2.8 μm. *Sensors* **2020**, *20*, 4642. [CrossRef]
11. Currey, R.; Khademian, A.; Shiner, D. Development of a Thulium Fiber Laser for an Atomic Spectroscopy Experiment. *Fibers* **2020**, *8*, 12. [CrossRef]
12. Tang, M.; Granger, G.; Lesparre, F.; Wang, H.; Qian, K.; Lecaplain, C.; Oudar, J.-L.; Jaouen, Y.; Gabet, R.; Gaponov, D.; et al. Large Normal Dispersion Mode-Locked Erbium-Doped Fiber Laser. *Fibers* **2019**, *7*, 97. [CrossRef]
13. Braunfelds, J.; Murnieks, R.; Salgals, T.; Brice, I.; Sharashidze, T.; Lyashuk, I.; Ostrovskis, A.; Spolitis, S.; Alnis, J.; Porins, J.; et al. Frequency comb generation in WGM microsphere based generators for telecommunication applications. *Quantum Electron.* **2020**, *50*, 1043–1049. [CrossRef]
14. Santos, D.; Guerreiro, A.; Baptista, J.M. Evaluation of Nanoplasmonic Optical Fiber Sensors Based on D-Type and Suspended Core Fibers with Metallic Nanowires. *Photonics* **2019**, *6*, 100. [CrossRef]
15. Cheng, T.; Zhang, F.; Tanaka, S.; Li, S.; Yan, X.; Zhang, X.; Suzuki, T.; Ohishi, Y. Ultrafast All-Optical Signal Modulation Induced by Optical Kerr Effect in a Tellurite Photonic Bandgap Fiber. *Photonics* **2019**, *6*, 113. [CrossRef]
16. Dudley, J.M.; Genty, G.; Coen, S. Supercontinuum generation in photonic crystal fiber. *Rev. Mod. Phys.* **2006**, *78*, 1135–1184. [CrossRef]
17. Okhrimchuk, A.G.; Pryamikov, A.D.; Gladyshev, A.V.; Alagashev, G.K.; Smayev, M.P.; Likhov, V.V.; Dorofeev, V.V.; Motorin, S.E.; Yatsenko, Y.P. Direct Laser Written Waveguide in Tellurite Glass for Supercontinuum Generation in 2 μm Spectral Range. *J. Lightwave Technol.* **2020**, *38*, 1492–1500. [CrossRef]
18. Knight, J.C.; Birks, T.A.; Russell, P.S.J.; Atkin, D.M. All-silica single-mode optical fiber with photonic crystal cladding. *Opt. Lett.* **1996**, *21*, 1547–1549. [CrossRef] [PubMed]
19. Zheltikov, A.M. Nonlinear optics of microstructure fibers. *Phys. Uspekhi* **2004**, *47*, 69. [CrossRef]

20. Litchinitser, N.M.; Dunn, S.C.; Usner, B.; Eggleton, B.J.; White, T.P.; McPhedran, R.C.; de Sterke, C.M. Resonances in microstructured optical waveguides. *Opt. Express* **2003**, *11*, 1243–1251. [CrossRef]

21. Price, J.H.V.; Monro, T.M.; Ebendorff-Heidepriem, H.; Poletti, F.; Horak, P.; Finazzi, B.; Leong, J.Y.Y.; Petropoulos, P.; Flanagan, J.C.; Brambilla, G.; et al. Mid-IR Supercontinuum Generation from Nonsilica Microstructured Optical Fibers. *IEEE J. Sel. Topics Quantum Electron.* **2007**, *13*, 738–748. [CrossRef]

22. Yatsenko, Y.P.; Kosolapov, A.F.; Levchenko, A.E.; Semjonov, S.L.; Dianov, E.M. Broadband wavelength conversion in a germanosilicate-core photonic crystal fiber. *Opt. Lett.* **2009**, *34*, 2581–2583. [CrossRef]

23. El-Amraoui, M.; Gadret, G.; Jules, J.C.; Fatome, J.; Fortier, C.; Désévédavy, F.; Skripatchev, I.; Messaddeq, Y.; Troles, J.; Brilland, L.; et al. Microstructured chalcogenide optical fibers from As_2S_3 glass: Towards new IR broadband sources. *Opt. Express* **2010**, *18*, 26655–26665. [CrossRef] [PubMed]

24. Domachuk, P.; Wolchover, N.A.; Cronin-Golomb, M.; Wang, A.; George, A.K.; Cordeiro, C.M.B.; Knight, J.C.; Omenetto, F.G. Over 4000 nm bandwidth of mid-IR supercontinuum generation in sub-centimeter segments of highly nonlinear tellurite PCFs. *Opt. Express* **2008**, *16*, 7161–7168. [CrossRef] [PubMed]

25. Bi, W.; Li, X.; Xing, Z.; Zhou, Q.; Fang, Y.; Gao, W.; Xiong, L.; Hu, L.; Liao, M. Wavelength conversion through soliton self-frequency shift in tellurite microstructured fiber with picosecond pump pulse. *J. Appl. Phys.* **2016**, *119*, 43102. [CrossRef]

26. Tao, G.; Ebendorff-Heidepriem, H.; Stolyarov, A.M.; Danto, S.; Badding, J.V.; Fink, Y.; Ballato, J.; Abouraddy, A.F. Infrared fibers. *Adv. Opt. Photonics* **2015**, *7*, 379–458. [CrossRef]

27. Nguyen, H.T.; Switkowski, K.; Filipkowski, A.; Kasztelanic, R.; Pysz, D.; Van Le, H.; Stepien, R.; Krolikowski, W.; Buczynski, R. Fiber microprobe with integrated gradient index vortex mask. *Opt. Commun.* **2020**, *477*, 126345. [CrossRef]

28. Bouwmans, G.; Bigot, L.; Quiquempois, Y.; Lopez, F.; Provino, L.; Douay, M. Fabrication and characterization of an all-solid 2D photonic bandgap fiber with a low-loss region (<20 dB/km) around 1550 nm. *Opt. Express* **2005**, *13*, 8452–8459. [CrossRef]

29. Klimczak, M.; Siwicki, B.; Skibiński, P.; Pysz, D.; Stępień, R.; Heidt, A.; Radzewicz, C.; Buczyński, R. Coherent supercontinuum generation up to 2.3 μm in all-solid soft-glass photonic crystal fibers with flat all-normal dispersion. *Opt. Express* **2014**, *22*, 18824–18832. [CrossRef]

30. Dong, L.; Thomas, B.K.; Fu, L. Highly nonlinear silica suspended core fibers. *Opt. Express* **2008**, *16*, 16423–16430. [CrossRef]

31. Mouawad, O.; Picot-Clemente, J.; Amrani, F.; Strutynski, C.; Fatome, J.; Kibler, B.; Desevedavy, F.; Gadret, G.; Jules, J.-C.; Deng, D.; et al. Multioctave midinfrared supercontinuum generation in suspendedcore chalcogenide fibers. *Opt. Lett.* **2014**, *39*, 2684–2687. [CrossRef]

32. Møller, U.; Yu, Y.; Kubat, I.; Petersen, C.R.; Gai, X.; Brilland, L.; Méchin, D.; Caillaud, C.; Troles, J.; Luther-Davies, B.; et al. Multi-milliwatt mid-infrared supercontinuum generation in a suspended core chalcogenide fiber. *Opt. Express* **2015**, *23*, 3282–3291. [CrossRef]

33. Anashkina, E.A.; Shiryaev, V.S.; Koptev, M.Y.; Stepanov, B.S.; Muravyev, S.V. Development of As-Se tapered suspended-core fibers for ultra-broadband mid-IR wavelength conversion. *J. Non Cryst. Solids* **2018**, *480*, 43–50. [CrossRef]

34. Karpate, T.; Stepniewski, G.; Pysz, D.; Rampur, A.; Stepanenko, Y.; Buczynski, R.; Klimczak, M. Soliton detuning of 68.5 THz in the near-infrared in a highly nonlinear suspended core tellurite fiber. *J. Opt. Soc. Am. B* **2020**, *37*, 1502–1509. [CrossRef]

35. Anashkina, E.A.; Dorofeev, V.V.; Skobelev, S.A.; Balakin, A.A.; Motorin, S.E.; Kosolapov, A.F.; Andrianov, A.V. Microstructured fibers Based on tellurite glass for nonlinear conversion of mid-IR ultrashort optical pulses. *Photonics* **2020**, *7*, 51. [CrossRef]

36. Liao, M.; Chaudhari, C.; Qin, G.; Yan, X.; Kito, C.; Suzuki, T.; Ohishi, Y.; Matsumoto, M.; Misumi, T. Fabrication and characterization of a chalcogenide-tellurite composite microstructure fiber with high nonlinearity. *Opt. Express* **2009**, *17*, 21608–21614. [CrossRef]

37. Ortiz, A.M.; Sáez, R.L. Multi-core optical fibers: Theory applications and opportunities. In *Selected Topics on Optical Fiber Technologies and Applications*; IntechOpen Limited: London, UK, 2017. [CrossRef]

38. Xia, C.; Bai, N.; Ozdur, I.; Zhou, X.; Li, G. Supermodes for optical transmission. *Opt. Express* **2011**, *19*, 16653–16664. [CrossRef]

39. Rubenchik, A.M.; Chekhovskoy, I.S.; Fedoruk, M.P.; Shtyrina, O.V.; Turitsyn, S.K. Nonlinear pulse combining and pulse compression in multi-core fibers. *Opt. Lett.* **2015**, *40*, 721–724. [CrossRef]

40. Turitsyn, S.K.; Rubenchik, A.M.; Fedoruk, M.P.; Tkachenko, E. Coherent propagation and energy transfer in low-dimension nonlinear arrays. *Phys. Rev. A* **2012**, *86*, 31804. [CrossRef]

41. Balakin, A.A.; Skobelev, S.A.; Anashkina, E.A.; Andrianov, A.V.; Litvak, A.G. Coherent propagation of laser beams in a small-sized system of weakly coupled optical light-guides. *Phys. Rev. A* **2018**, *98*, 43857. [CrossRef]

42. Balakin, A.A.; Skobelev, S.A.; Andrianov, A.V.; Anashkina, E.A.; Litvak, A.G. Coherent propagation and amplification of intense laser pulses in hexagonal multicore fibers. *Opt. Lett* **2020**, *45*, 3224–3227. [CrossRef]

43. Andrianov, A.V.; Kalinin, N.A.; Anashkina, E.A.; Egorova, O.N.; Lipatov, D.S.; Kim, A.V.; Semjonov, S.L.; Litvak, A.G. Selective excitation and amplification of peak-power-scalable out-of-phase supermode in Yb-doped multicore fiber. *J. Light. Technol.* **2020**, *38*, 2464–2470. [CrossRef]

44. Balakin, A.A.; Litvak, A.G.; Skobelev, S.A. Stability of out-of-phase solitons and laser pulse self-compression in active multicore fibers. *Phys. Rev. A* **2019**, *100*, 53834. [CrossRef]

45. Chiang, K.S. Intermodal dispersion in two-core optical fibers. *Opt. Lett.* **1995**, *20*, 997–999. [CrossRef] [PubMed]

46. Peterka, P.; Honzatko, P.; Kanka, J.; Matejec, V.; Kasik, I. Generation of high-repetition-rate pulse trains in a fiber laser through a twin-core fiber. In *Photonics, Devices, and Systems II, Proceedings of the SPIE, Prague, Czech Republic 26–29 May 2002*; SPIE: Bellingham, DC, USA, 2003; Volume 5036, pp. 376–381. [CrossRef]

47. Benton, C.J.; Skryabin, D.V. Coupling induced anomalous group velocity dispersion in nonlinear arrays of silicon photonic wires. *Opt. Express* **2009**, *17*, 5879–5884. [CrossRef]

48. De Nobriga, C.E.; Hobbs, G.D.; Wadsworth, W.J.; Knight, J.C.; Skryabin, D.V.; Samarelli, A.; Sorel, M.; De La Rue, R.M. Supermode dispersion and waveguide-to-slot mode transition in arrays of silicon-on-insulator waveguides. *Opt. Lett.* **2010**, *35*, 3925–3927. [CrossRef]

49. Peterka, P.; Kasik, I.; Kanka, J.; Honzatko, P.; Matejec, V.; Hayer, M. Twin-core fiber design and preparation for easy splicing. *IEEE Photonics Technol. Lett.* **2000**, *12*, 1656–1658. [CrossRef]

50. Castro, C.; Jain, S.; De Man, E.; Jung, Y.; Hayes, J.; Calabro, S.; Pulverer, K.; Bohn, M.; Alam, S.; Richardson, D.J.; et al. 100-Gb/s transmission over a 2520-km integrated MCF system using cladding-pumped amplifiers. *IEEE Photonics Technol. Lett.* **2017**, *29*, 1187–1190. [CrossRef]

51. Liu, Z.; Zhang, Z.F.; Tam, H.Y.; Tao, X. Multifunctional smart optical fibers: Materials, fabrication, and sensing applications. *Photonics* **2019**, *6*, 48. [CrossRef]

52. Bookey, H.T.; Lousteau, J.; Jha, A.; Gayraud, N.; Thomson, R.R.; Psaila, N.D.; Li, H.; MacPherson, W.N.; Barton, J.S.; Kar, A.K. Multiple rare earth emissions in a multicore tellurite fiber with a single pump wavelength. *Opt. Express* **2007**, *15*, 17554–17561. [CrossRef]

53. Cheng, T.; Duan, Z.; Gao, W.; Asano, K.; Liao, M.; Deng, D.; Suzuki, T.; Ohishi, Y. A novel seven-core multicore tellurite fiber. *J. Light. Technol.* **2013**, *31*, 1793–1796. [CrossRef]

54. Cheng, T.; Duan, Z.; Liao, M.; Gao, W.; Deng, D.; Suzuki, T.; Ohishi, Y. A simple all-solid tellurite microstructured optical fiber. *Opt. Express* **2013**, *21*, 3318–3323. [CrossRef] [PubMed]

55. Dorofeev, V.V.; Moiseev, A.N.; Churbanov, M.F.; Kotereva, T.V.; Chilyasov, A.V.; Kraev, I.A.; Pimenov, V.G.; Ketkova, L.A.; Dianov, E.M.; Plotnichenko, V.G.; et al. Production and properties of high purity TeO_2–WO_3–(La_2O_3, Bi_2O_3) and TeO_2–ZnO–Na_2O–Bi_2O_3 glasses. *J. Non Cryst. Solids* **2011**, *357*, 2366–2370. [CrossRef]

56. Boivin, M.; El-Amraoui, M.; Ledemi, Y.; Morency, S.; Vallée, R.; Messaddeq, Y. Germanate-tellurite composite fibers with a high-contrast step-index design for nonlinear applications. *Opt. Mater. Express* **2014**, *4*, 1740–1746. [CrossRef]

57. Anashkina, E.A.; Dorofeev, V.V.; Koltashev, V.V.; Kim, A.V. Development of Er^{3+}-doped high-purity tellurite glass fibers for gain-switched laser operation at 2.7 μm. *Opt. Mater. Express* **2017**, *7*, 4337–4351. [CrossRef]

58. Kedenburg, S.; Strutynski, C.; Kibler, B.; Froidevaux, P.; Désévédavy, F.; Gadret, G.; Jules, J.-C.; Steinle, T.; Mörz, F.; Steinmann, A.; et al. High repetition rate mid-infrared supercontinuum generation from 1.3 to 5.3 μm in robust step-index tellurite fibers. *J. Opt. Soc. Am. B* **2017**, *34*, 601–607. [CrossRef]

59. Snyder, A.W.; Love, J. *Optical Waveguide Theory*; Chapman and Hall: New York, NY, USA, 1983.